Microstructure and thermal stability of superplastic aluminium—lithium alloy after severe plastic deformation

A. A. MAZILKIN*, M. M. MYSHLYAEV
Institute of Solid State Physics, Russian Academy of Sciences, Chernogolovka, Moscow District, 142432, Russia
E-mail: mazilkin@issp.ac.ru

Published online: 10 April 2006

Structure and phase composition of 1420 (Al-Mg-Li-Zr) alloy obtained by equal channel angular pressing during mechanical tensile testing and annealing within the temperature range 423–723 K were studied by means of TEM and XRDA. It was revealed that structural changes of the alloy after the mechanical tests corresponded to two stages of the deformation. The alloy structure was unstable due to its non-equilibrium nature and came to the equilibrium state during the annealing. Changes in the grain size and phase composition during the alloy annealing resulted in a significant decrease of its hardness.

1. Introduction

Modern techniques of the severe plastic deformation such as high pressure torsion [1, 2] equal channel angular pressing (ECAP) [3, 4], accumulative roll-bonding [5, 6] were recently developed and successfully applied to obtain an ultra-fine grain (UFG) structure in a various materials. The advantage of these techniques is that they allow producing fine-grain structure without changing the initial dimension of the original sample. The ultra-fine grain structure determines extraordinary properties of such materials. For instance the phenomenon of high strain rate superplasticity was demonstrated recently for the UFG aluminium-based alloys after the ECAP deformation [7–9]. Another important condition to be held for this phenomenon is the ability of the material to maintain its structure during the heating as the superplasticity is observed at elevated temperatures (usually at $T \sim 0.5\ T_m$ and higher, T_m being the melting point) [10]. However, UFG materials are characterized by high internal stresses and non equilibrium structure features. All these factors make them sensitive to the thermal treatment and restrict significantly their commercial application.

The aim of this work is to study the structure in superplastic aluminium-based alloy formed by ECAP, its evolution during deformation and also its stability in the course of heat treatment.

2. Experimental

The study was carried out on the 1420 aluminium alloy (Al-5.5 wt.% Mg-2.2 wt.% Li-0.12 wt.%. Zr) preprocessed by the ECAP. Detailed description of this deformation technique may be found elsewhere [2, 3, 11]. The ECAP processing was carried out at 643 K. Ten passages through the die were done and the sample was rotated by 90° round its axis in the same direction before each passage. The rotation allows obtaining homogeneous microstructure in the alloy [11]. The produced material was tested by axial tension with the initial strain rate 10^{-2} s^{-1} at 623 K. Samples exhibited superplastic flow during the tests with the largest elongation about 1900%. Thermal stability of the 1420 alloy after the ECAP was investigated by the annealing of the alloy samples at 423, 523, 623 and 723 K during 0.5, 1, 2 and 3 h respectively. Structure and phase composition of the alloy were investigated by the transmission electron microscopy (TEM) and X-rays diffraction analysis (XRDA). JEM-100CX and JEM-4000FX electron microscopes were used for TEM investigations. The latter was equipped by the system of energy dispersive X-rays (EDX) analysis with a high-purity Ge detector. Characteristics of subboundaries (structure, types of the dislocations) were determined by $g{\cdot}b$ and trace analysis [12] (g and b being diffraction and Burgers vectors respectively).

*Author to whom all correspondence should be addressed.
0022-2461
DOI: 10.1007/s10853-006-2637-4

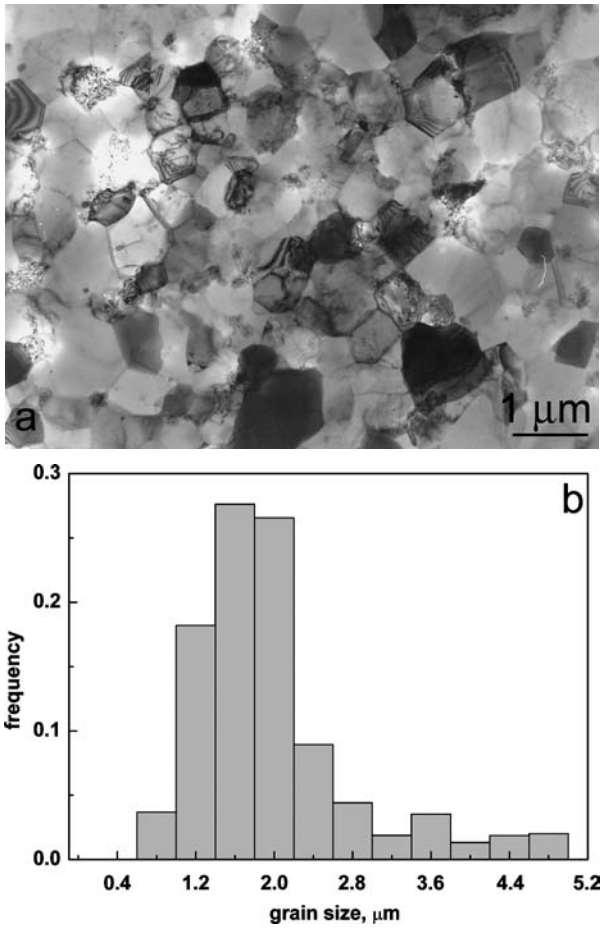

Figure 1 Structure (a) and grain size distribution (b) of 1420 aluminium alloy after ECAP.

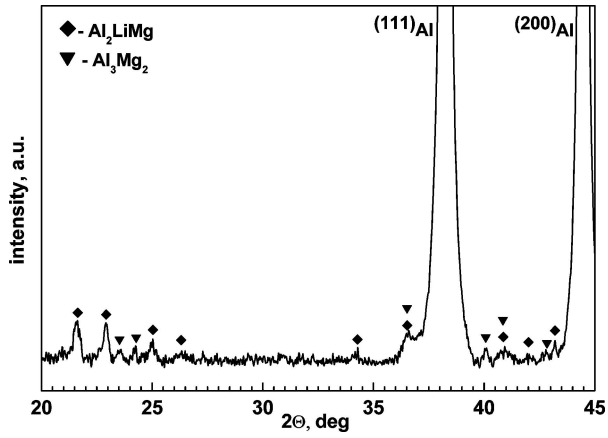

Figure 2 X-rays diffraction data for 1420 alloy after ECAP. Reflections from Al_2LiMg and Al_3Mg_2 phases and aluminium are indicated.

XRDA experiments were carried out on the SIEMENS-500 diffractometer with Cu K_α radiation. Vickers microhardness was determined in order to characterize change in mechanical properties of the alloy during annealing. The measurements were done with the load value of 50 g.

3. Results and discussion

Mean grain size in the initial state of the alloy after the ECA pressing is 1.6 μm (Fig. 1).The grain size distribution was plotted on the base of TEM images. Grains have equiaxial shape. Inside the grains there exists a developed substructure characterized by the presence of individual dislocations, pile-ups of dislocations and dislocation subboundaries. The average dislocation density is about 10^9 cm^{-2}. Particles of S_1 (Al_2LiMg) phase have been detected in the structure. S_1-phase is precipitated as colonies at grain boundaries, in grain boundaries junctions and also inside the grains. The colony size is about 0.2–0.3 μm. This phase has been revealed by XRDA as well (Fig. 2). There are also reflections from another phase in this spectrum which correspond to Al_3Mg_2 compound. δ' (Al_3Li) and β' (Al_3Zr) phases can also present in the studying alloy according to [13, 14]. Particles of δ'-phase are dispersed and revealed by their reflections in diffraction patterns.

Set of photographs illustrates changes in the alloy structure after different degrees of tensile deformation (Fig. 3). It has been mentioned above that equiaxial grain structure was a distinctive feature of the initial state of the alloy. In samples deformed to $\varepsilon = 110\%$ and 300% (Fig. 3a and b) predominance of extended grains is noticeable. Samples subjected to higher degrees of deformation (900 and 1200%) exhibited the structure, in which the equiaxial grains are observed again (Fig. 3c and d). Herewith the average grain size increases slightly. The dislocation density decreases to 10^6–10^7 cm^{-2}. There are no visible changes in size, shape and relative volume fraction of Al_2LiMg particles.

The obtained results indicate the existence of at least two stages of deformation of the microcrystalline 1420 Al-Li alloy. This agrees with the data on its mechanical behaviour [9]. The conclusion of multistage character of plastic deformation was done by examining true stress – true strain dependence. The first stage is that of hardening which is followed by the softening one. For these two stages the activation energy was determined. For hardening stage the activation energy was equal to 1.4 eV, for softening one it was 1 eV. Using these activation energy values, mechanisms controlled the superplastic deformation were suggested. In the first stage the deformation is supposed to be controlled by self-diffusion in the grain bulk that corresponds to the intragranular dislocation slide. In the second stage, it is the self-diffusion along the grain boundaries that corresponds to the grain boundary sliding.

The study of the grain structure evolution of the alloy confirms validity of the conclusions concerning the deformation controlling mechanisms. It was observed that in the first stage ($\varepsilon = 110\%$ and 300%) the structure consisted mainly of extended grains. The density of dislocations inside the grains in this deformation stage is rather high. These structural features indicate that the most probable deformation mechanism is the intragranular gliding

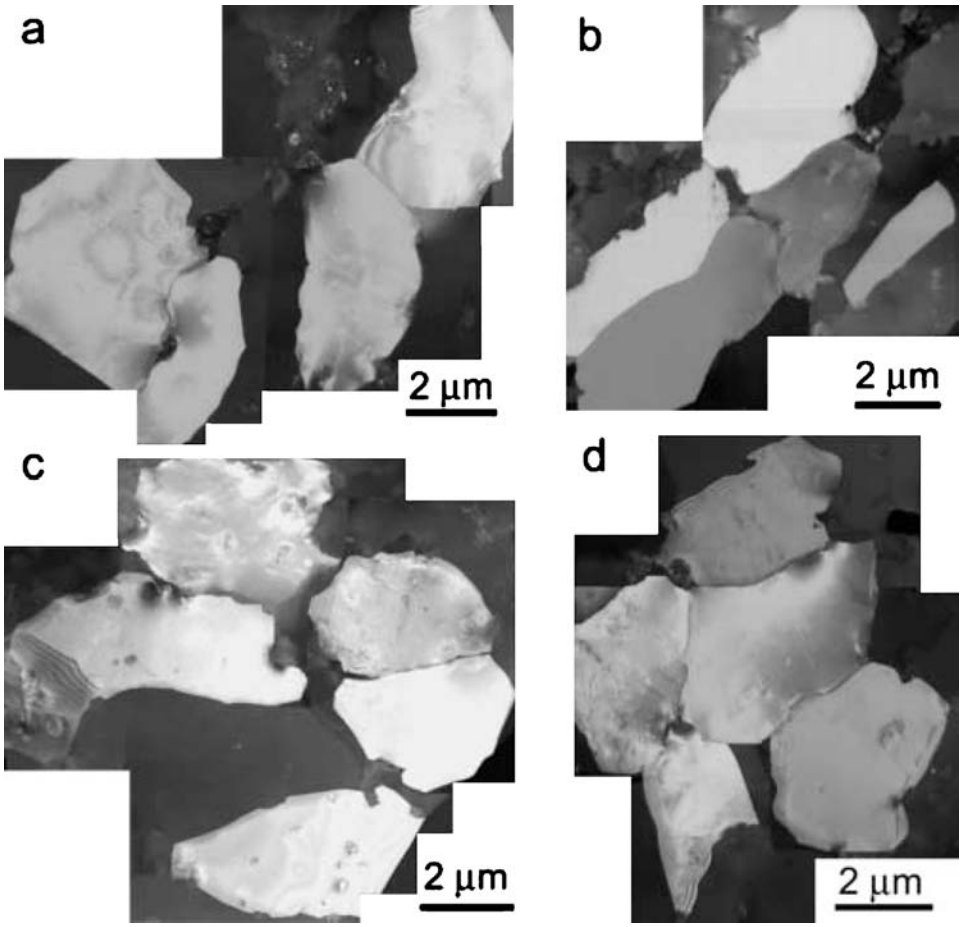

Figure 3 Structure of the alloy in the course of tensile tests: $\varepsilon = 110\%$ (a), 300% (b), 900% (c), 1200% (d).

of dislocations. The observations of alloy structure in the softening stage ($\varepsilon = 900\%$ and 1200%) showed that grain gained equiaxial shape but the dislocation density decreased significantly, i.e. it would be quite correct to expect that the deformation in this stage is controlled by grain boundary sliding.

The structure of dislocation subboundaries observed inside the grains was investigated in detail. It should be noted that subboundary structure was rather regular though it was formed during severe plastic deformation. It obviously indicates that along with the dislocation glide the non-conservative processes also took an active part in forming of the subboundaries. Examples of two such subboundaries are represented in Fig. 4.

The subboundary in Fig. 4a is a tilt dislocation wall. Foil area corresponded to the grain in which the wall is situated coincides with the (110) plane. By the trace analysis the plane subboundary was determined to be parallel to (021). The technique of $g{\cdot}b$-analysis allowed to determine that the Burgers vector is $a/2[110]$; unit vector along the dislocation line is parallel to the $[1\bar{1}2]$ direction. Therefore the wall consists of gliding mixed dislocations, and the angle between the Burgers vector and the dislocation line is $\sim 55^\circ$. Fig. 4b demonstrates another type of subboundary. It is a hexagonal dislocation network formed by dislocations of three families. Using the same procedure as in previous case it has been determined that the plane of the subboundary is parallel to (111) crystallographic plane. In order to determine the Burgers vectors the value of $g{\cdot}[b{\times}u]$ product was calculated [12]. The dislocation Burgers vectors and corresponding unit vectors along the dislocation lines were $b_1 = a/2[101]$, $u_1 = [10\bar{1}]$, $b_2 = a/2[\bar{1}10]$, $u_2 = [1\bar{5}4]$, and $b_3 = a/2[011]$, $u_1 = [3\bar{5}1]$ correspondingly. The Burgers vectors also meet the requirements to be equal to zero in the point of the dislocations intersection. All the dislocations being included in the network are mixed with a significant edge component.

The results of TEM studies of dislocation subboundaries showed that mainly non-equilibrium subboundaries of different kind constituted the substructure of the grains. The non-equilibrium character of subboundaries may be caused by various reasons. First, it is irregularity in their structure. Second, it is because the walls formed by the dislocations with a high screw component and nets included dislocations with a significant edge component generate long-range stress fields and are unstable [15]. It has been shown both during conventional annealing and by *in-situ* heating experiments that such non-equilibrium

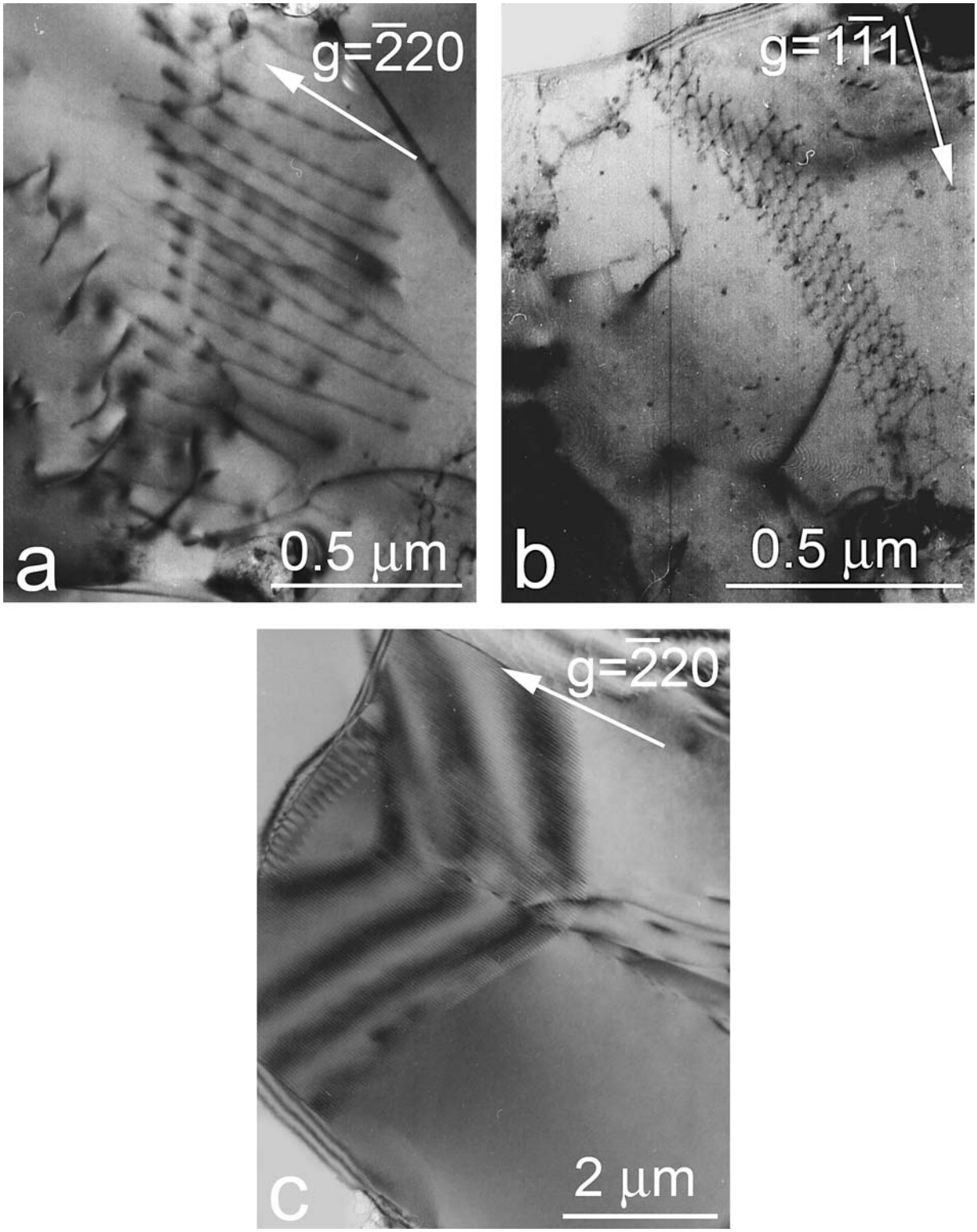

Figure 4 Microphotographs of the dislocation subboundaries: (a) dislocation wall; (b) dislocation network; (c) dislocation wall consisted of edge dislocations.

subboundaries with increased energy suffer thermoactivated destruction. Then, walls of straight edge sessile dislocations with minimal free energy are mainly observed in substructure after the heating up to 623 K like in Fig. 4c where the dislocations have Burgers vector $b_2 = a/2[101]$ and the angle between the Burgers vector and the dislocation line is 90°.

Annealing causes decreasing of the dislocation density and change in the grain structure. Changes of phase composition are also observed. Fig. 5 demonstrates grain size

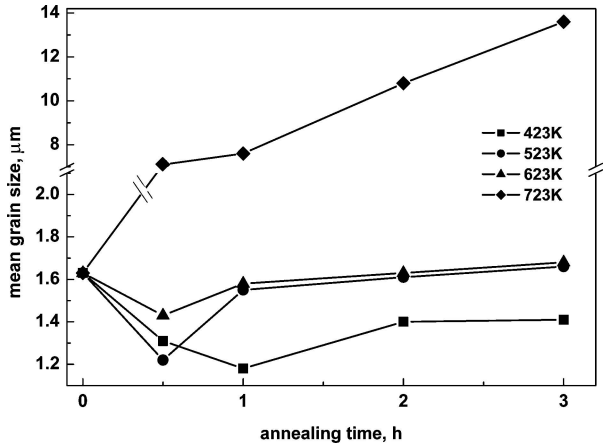

Figure 5 Time dependences of the mean grain size at different annealing temperatures.

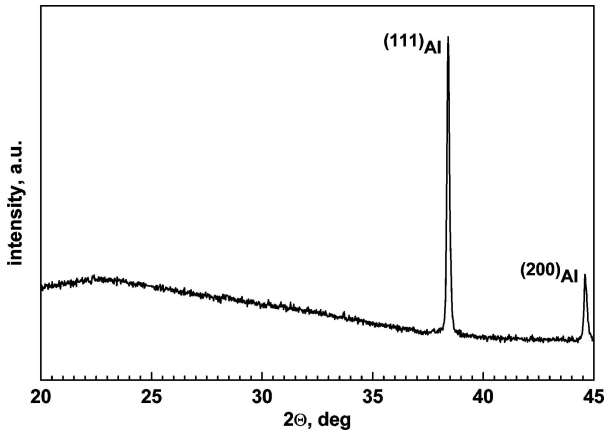

Figure 6 X-rays diffraction data for 1420 alloy after ECAP deformation and annealing at 723 K during 1 h.

dependences in the course of annealing. Decreasing of the grain size is noticeable for $T = 423$–623 K and the annealing time 0.5–1 h. Such behaviour could be explained by the formation of new grain boundaries from subgrain boundaries and dislocations inserted in the materials due to the previous deformation. During the annealing grains maintain the equiaxial shape and their size is increased but only slightly exceeds the value obtained after the ECAP deformation. Colonies of S_1-phase are observed in the structure. The histograms plotted for the annealed alloy samples revealed that the grain structure at 423–623 K and all durations is characterized by normal size distribution. Significant grain growth takes place during the annealing at the temperature 723 K. The microstructure contains both large recrystallized grains and those with the size close to the initial (before annealing) state. Change in the alloy phase composition takes place at this temperature. According to the TEM investigations which are also supported by the XRDA data, there are no precipitations of the S_1-phase in the alloy (Fig. 6). Instead globular particles of about 0.5–1.5 μm in size are observed (Fig. 7a). According to [16] at temperature ~630 K the metastable δ'-phase has to be substituted by stable δ-phase (AlLi).

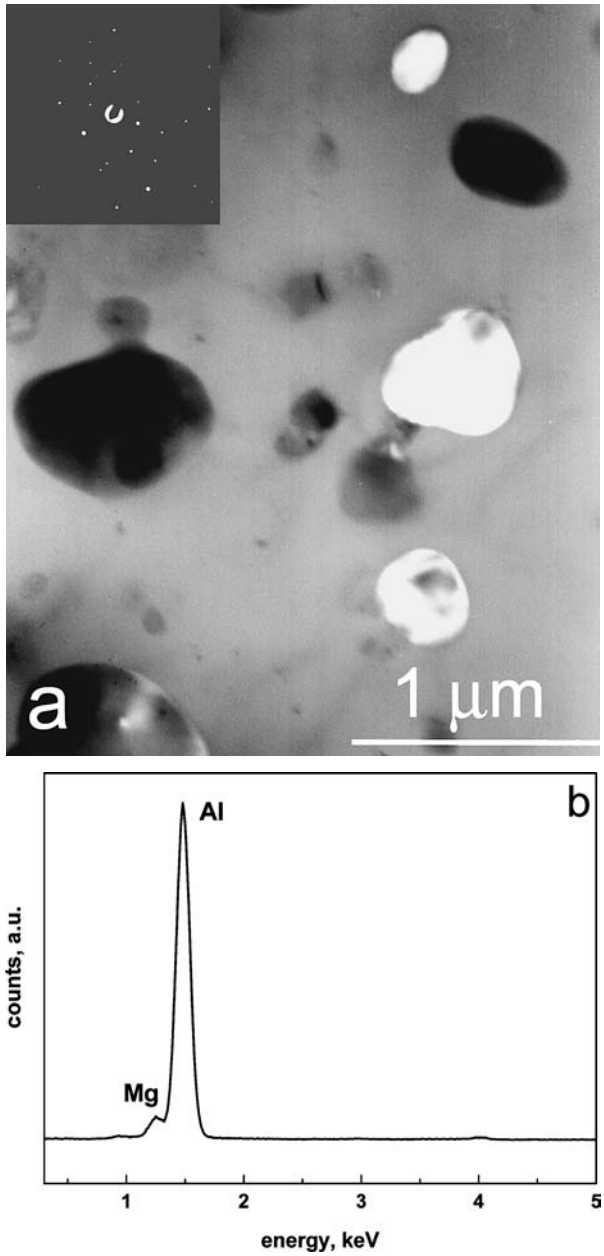

Figure 7 Dark field image with a selected area diffraction pattern (a) and EDX-spectrum (b) of δ-phase particles in 1420 alloy; annealing at 723 K during 1 h.

Hence, the observed particles can be the precipitations of δ or β' (Al_3Zr) phases. Analysis of the reflections in electron diffraction pattern showed that they correspond to δ-phase. This conclusion is confirmed by EDX analysis of the particles. Fig. 7b represents the EDX spectrum corresponding to particle area in the investigated alloy after 1 h annealing at 723 K. It can be seen from this plot that only the peaks of aluminium and magnesium are observed and there is no sign of zirconium. Taking into account that this method is not able to reveal the presence of light elements (e.g. lithium) we can conclude that the precipitations belong to δ-phase.

Behaviour of the Vickers microhardness correlates with the changes in microstructure (Fig. 8). Microhardness

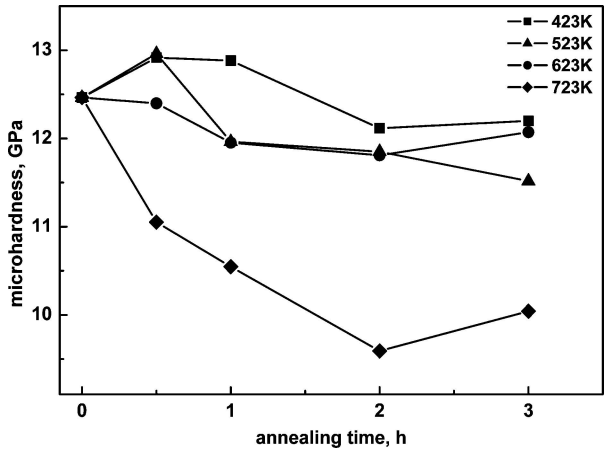

Figure 8 Time dependences of the Vickers microhardness.

practically does not change for the annealing at 523 and 623 K. Certain increase of the hardness value at 0.5 h corresponds to the observed reduction of the grain size. Microhardness reduces significantly (∼30%) during the annealing at 723 K. This drop can be caused by at least two reasons. First, it is a substantial grain growth. The second one is the change in phase composition of the alloy. It is known that the strengthening in Al-Li-Mg system is determined both by δ' and S_1-phases [14]. Annealing at 723 K resulted in disappearance of the S_1-phase and δ'-phase is substituted by the stable δ-phase which has no impact on the strength of the material [14].

4. Conclusions

1. Structural changes in 1420 aluminium alloy during tensile tests revealed existence of two deformation stages with different deformation mechanisms. These are hardening stage with intragranular dislocation sliding and softening stage with grain boundary sliding mechanism. Substructure of the alloy is characterized by the presence of subboundaries with a substantially non-equilibrium nature.

2. Structure and mechanical properties of the 1420 alloy are proved to be stable during the thermal treatment up to 623 K. Annealing at high temperature leads to the substantial grain growth and change of the alloy phase composition.

Acknowledgments

The financial support from the Russian Foundation for Basic Researches (Projects No. 03-02-16947, 04-02-97261, 04-02-16129) is greatly appreciated.

References

1. I. V. ALEXANDROV, Y. T. ZHU, T. C. LOWE and R. Z. VALIEV, *Powder Metall.* **41** (1998) 11; (1994) 1631.
2. B. B. STRAUMAL, B. BARETZKY, A. A. MAZILKIN, F. PHILLIPP, O. A. KOGTENKOVA, M. N. VOLKOV and R. Z. VALIEV, *Acta Materialia* **52** (2004) 4469.
3. V. M. SEGAL, *Mater. Sci. Eng. A* **197** (1995) 157.
4. R. Z. VALIEV, N. A. KRASILNIKOV and N. K. TSENEV, *Mater. Sci. Eng. A* **137** (1991) 35.
5. K. PARK, H. KWON, W. KIM and Y. KIM, *ibid.* **316** (2001) 145.
6. N. TSUJI, Y. SAITO, H. UTSUNOMIYA and S. TANIGAWA, *Scripta Mater.* **40** (1999) 795.
7. R. Z. VALIEV, D. A. SALIMONENKO, N. K. TSENEV, P. B. BERBON and T. G. LANGDON, *ibid.* **37** (1997) 1945.
8. S. KOMURA, P. B. BERBON, M. FURUKAWA, Z. HORITA, M. NEMOTO and T. G. LANGDON, *ibid.* **38** (1998) 1851.
9. M. M. MYSHLYAEV, V. V. SHPEIZMAN and M. M. KAMALOV, *Phys. Sol. State* **43** (2001) 2099.
10. T. G. LANGDON, *Metall. Trans.* **13A** (1982) 689.
11. M. FURUKAWA, Y. IWAHASHI, Z. HORITA, M. NEMOTO and T. G. LANGDON, *Mat. Sci. Eng. A* **257** (1998) 328.
12. "Electron Microscopy of Thin Crystals", edited by P. B. Hirsch, A. Howie, R. B. Nicholson, D. W. Pashley and M. J. Whelan, (Butterworths, London, 1965).
13. T. B. MASSALSKI *et al.* (eds.), "Binary Alloy Phase Diagrams". (ASM International, Materials Park, OH, 1993) p. 127.
14. J. N. FRIDLYANDER, K. V. CHUISTOV, A. L. BERESINA and N. I. KOLOBNEV, Aluminum—Lithium Alloys (Structure and Properties), (Naukova Dumka, Kiev, 1992) p. 192.
15. J. C. M. LI, in "Electron Microscopy and Strength of Crystals" edited by G. Thomas and J. Washburn (N.Y., 1963) p. 713.
16. S. SEREZARA, G. COCCO, G. FAGHERAZZI and L. SCHIFFINI, *Phil. Mag.* **35** (1977) 378.

Received 21 February
and accepted 27 May 2005